



1 **Effects of Anthropogenic Pollutants on Biogenic Secondary**
2 **Organic Aerosol Formation in the Atmosphere of Mt. Hua,**
3 **China**

4 Can Wu^{1,2}, Yubao Cheng¹, Yuwei Sun¹, Huijun Zhang¹, Si Zhang¹, Cong Cao^{3*},
5 Jianjun Li³, Gehui Wang^{1,2*}
6
7
8

9 ¹Key Lab of Geographic Information Science of the Ministry of Education, School of
10 Geographic Sciences, East China Normal University, Shanghai 210062, China

11 ²Institute of Eco-Chongming, 3663 North Zhongshan Road, Shanghai 200062, China

12 ³State Key Laboratory of Loess and Quaternary Geology, Institute of Earth
13 Environment, Chinese Academy of Sciences, Xi'an 710061, China

14 *Now at Department of Chemistry, Hong Kong University of Science & Technology
15
16
17
18
19
20
21
22
23
24
25
26
27
28
29
30
31
32

33 *Corresponding author. Por. Gehui Wang,
34 Mailing address: School of Geographic Sciences, East China Normal University,
35 Shanghai 210062, China
36 E-mail address: ghwang@geo.ecnu.edu.cn, or wanggh@ieecas.cn (Gehui Wang)
37
38



39 **Abstract:** Anthropogenic effects on biogenic secondary organic aerosol (BSOA)
40 formation in the upper boundary layer are still not fully understood. Here, A
41 synchronized 4-hourly monitoring of three typical BSOA tracers from isoprene,
42 monoterpenes, β -caryophyllene and other particulate pollutants was conducted at the
43 mountain foot (MF, 400 m a.s.l.) and mountainside (MS, 1120 m a.s.l.) of Mt. Hua,
44 China, to investigate the chemical evolution of BSOA in air mass lifting. Our
45 findings revealed that BSOA was the predominant source of organic matter (OM) at
46 MS site, with an average fraction of ~43% being ~7-fold of that at MF site. As the
47 prevalent BSOA tracer, isoprene-derived SOA tracers (BSOA_I) maintained
48 comparable level at MF site (182.5 ± 81 ng/m³) and MS site (197.3 ± 127 ng/m³), yet
49 exhibited an inverse diurnal pattern between both sites. And the BSOA_I fraction in
50 OM aloft moderately decreased during the daytime, and correlated positively with 2-
51 methyltetrols/2-methylglyceric acid ratio but negatively with NO_x transported from
52 ground level, indicating that anthropogenic NO_x would significantly affect the
53 daytime BSOA formation aloft by inhibiting the HO₂[·]-pathway products. Additionally,
54 the further formation of sulfate in lifting air mass would significantly enhance aerosol
55 water content aloft, which suppressed the reactive uptake of isoprene epoxydiol and
56 ultimately diminished the BSOA_I yields during the daytime. These findings provide
57 more insight into the intricate anthropogenic–biogenic interactions affecting BSOA
58 formation in the upper boundary layer atmosphere.

59 **Keywords:** Biogenic Secondary Organic Aerosol; Isoprene; Anthropogenic pollutants;
60 Vertical distribution



61 **1. Introduction**

62 Volatile organic compounds (VOCs) play a crucial role in atmospheric chemistry
63 (Mcfiggans et al., 2019; Coggon et al., 2021), exerting profound influences on the
64 atmospheric oxidizing capacity, tropospheric ozone burden and regional climate
65 (Mellouki et al., 2015; Wu et al., 2020). Among the diverse VOCs, biogenic VOCs
66 (BVOCs) primarily emitted by terrestrial vegetation predominate the global VOC flux
67 at 1Pg/yr (Guenther et al., 2012), exceeding anthropogenic sources by an order of
68 magnitude. The high reactivity of dominant BVOCs (particularly, isoprene,
69 monoterpene, and sesquiterpenes) towards O_3 , $OH\cdot$ and $NO_3\cdot$ would drive rapid
70 formation of secondary organic aerosol (SOA) (Zhang et al., 2018; Ng et al., 2017).
71 Consequently, these biogenically-derived SOA (BSOA) would represent a prominent
72 contribution to global SOA budget (Kelly et al., 2018; Hodzic et al., 2016), although
73 the models remain highly uncertain in BSOA prediction owing to the complexity of
74 physicochemical processes involved (Hallquist et al., 2009). Given the significant
75 climate interactions and public health implications of BSOA (Scott et al., 2014;
76 Shrivastava et al., 2017), advancing the understanding of BSOA, including its
77 precursors, formation processes, is urgently needed.

78 Over past two decades, mounting evidences indicate that anthropogenic pollutants
79 (e.g., SO_2 , NO_x) critically regulate the BSOA formation through altering oxidation
80 pathways and gas-to-particle partitioning processes (Xu et al., 2015; Zheng et al.,
81 2023; Xu et al., 2016). For example, sulfate aerosol formed by heterogeneous
82 reactions of SO_2 would influence particle acidity and water content (Wang et al., 2016;



83 Wang et al., 2025), which accelerates SOA formation by the “salting-in” effect and
84 corresponding acid-catalyzed reactions (Offenberg et al., 2009; Xu et al., 2016). NO_x
85 as an important driver for BSOA formation could modulate the fate of peroxy radicals
86 (RO₂·), and subsequently affect the yield and chemical composition of BVOC-
87 oxidized products (Lin et al., 2013; Pye et al., 2010). Abundant O₃ could also
88 significantly promote BSOA formation via enhancing BVOCs ozonolysis. Thus, the
89 changes of anthropogenic emissions would potentially perturb the BSOA formation.
90 As modeling studies demonstrated, anthropogenic emission controls substantially
91 decreased the BSOA formation in the United States during 1990–2012 (Ridley et al.,
92 2018), and ~ a further 35% of isoprene-derived SOA (SOA_I) would be reduced in
93 2025 if ongoing the similar emission regulations (Marais et al., 2016). The parallel
94 effects also emerged in China, where the effective control on SO₂ emissions drove a
95 significant decline of SOA_I at −8.0%/yr over 2007–2015, even being two-fold that of
96 SO₄^{2−} (Dong et al., 2022).

97 Numerous studies have comprehensively characterized the surface BSOA, yet the
98 vertical distribution of BSOA remains insufficiently understood, which is a critical
99 driver of uncertainties in the global climate models (Nazarenko et al., 2017;
100 Hodnebrog et al., 2014). The mountain-based observations revealed that BSOA
101 constitutes a substantial fraction (30–60%) of aerosols in free troposphere (Fu et al.,
102 2014; Ren et al., 2019; Yi et al., 2021); And these elevated BSOA are significantly
103 influenced by the valley breeze that would transport the surface pollutants to upper
104 boundary layer, indicating a potential effect of surface pollutant emissions on BSOA



105 formation aloft. In addition, airborne pollutants likely undergo aging in the vertical
106 transport process (Wu et al., 2022), causing increasingly complex compositions and
107 changes in oxidizing capacity and aerosol properties compared with that at ground
108 level. Consequently, more observations studies are necessary to obtain an improved
109 understanding of the anthropogenic–biogenic interactions driving BSOA formation
110 aloft.

111 Guanzhong Basin of inland China is a typical semiarid region in East Asia,
112 suffering serious particle pollution due to the large anthropogenic emissions (Wang et
113 al., 2016). In our previous studies (Li et al., 2013; Wang et al., 2012), the molecular
114 distribution, evolutionary mechanism and sources of BSOA have been investigated;
115 Whereas, the anthropogenic emissions experienced dramatical changes recently in this
116 region (Zhang et al., 2019a), thereby, the primary factors currently driving the BSOA
117 formation are probably distinct from those that prevailed previously. To elucidate the
118 formation mechanism of biogenic SOA aloft in this region, synchronous observations
119 were conducted on the mountainside and the mountain foot of Mt. Hua, adjoined the
120 Guanzhong basin. In this study, we firstly investigate chemical molecular
121 compositions and diurnal variation of the of BSOA over Mt. Hua, then explored the
122 impacts of anthropogenic pollutants on BSOA formation during the vertical transport,
123 and finally quantified its source contributions.

124 **2 Experiment**

125 **2.1 Sample collection**

126 From 27 August to 17 September 2016, aerosol sampling with 4-hr interval were



127 synchronously conducted at two locations in Mt. Hua region, employing the high-
128 volume air samplers with a flow rate of 1.13 m³/min. One sampling site (34°32'N,
129 110°5'E, 400 m a.s.l; MF) is situated at the mountain foot of Mt. Hua, enveloped by
130 several traffic arteries, residential and commercial buildings. Another site is located
131 on mountainside (34°29'N, 110°3'E, 1120 m a.s.l; MS), approximately 8 km away
132 from MF site in horizontal distance; This site is adjacent to one of the larger valleys of
133 Mt. Hua, characterized by precipitous terrain and less anthropogenic activities. The
134 surface-level pollutants can be transported to here by the prevailing valley breeze,
135 which has been validated by the organic tracers and meteorological field simulated by
136 WRF-Chem model in our previous studies (Wu et al., 2022; Wu et al., 2024). All the
137 aerosol samples were collected on pre-combusted quartz filters (450 °C for 6 hr), and
138 stored in a freezer (< -18 °C) prior to chemical analysis.

139 Additionally, the hourly concentration of the pollutants, including PM_{2.5}, O₃, NO₂,
140 were also monitored at MS site by corresponding online equipment; While, those data
141 for MF site were mainly acquired through Weinan Ecological Environment Bureau
142 (<http://sthjj.weinan.gov.cn/>, last access: 8 July 2021). All meteorological data were
143 downloaded from the Shaanxi Meteorological Bureau website (<http://sn.cma.gov.cn/>,
144 last access: 8 July 2021). The comprehensive details regarding the sampling sites and
145 instrumentation were delineated in our previous studies (Wu et al., 2022; Wu et al.,
146 2024).

147 **2.2 Chemical analysis**

148 The details of organic matter extraction, derivatization, and gas



149 chromatography/mass spectrometry (GC/MS) analyses can refer to elsewhere (Wang
150 and Kawamura, 2005). Briefly, for the analytical procedure of organic tracers in the
151 aerosol, one-quarter of PM_{2.5} sample was cut into pieces and then ultrasonically
152 extracted with a mixture of dichloromethane and methanol (2: 1, v/v) three times
153 (each for 15 min). The extracts were filtered through a pasteur pipette plugged with
154 quartz wool into a pear-shaped bottle. The filtrates were concentrated by a rotary
155 evaporator under vacuum state and then dried by pure nitrogen. After reaction with 60
156 Ml derivatization reagent (a mixture of 50 Ml of N,O-bis-
157 (trimethylsilyl)trifluoroacetamide (BSTFA) and 1 % trimethylsilyl chloride and 10 Ml
158 of pyridine) for 3 h at 70 °C in order to convert COOH and OH groups to the
159 corresponding trimethylsilyl esters and ethers. After cooling down to room
160 temperature, an aliquot of 40 Ml internal standard (C₁₃ n-alkene) was added into the
161 derivative solution prior to GC/MS analyses. The blank filters were also analyzed
162 following the same analytical procedure for the ambient samples.

163 Furthermore, partial filters were cut into pieces, and then extracted three times
164 under sonication with 15ml Milli-Q pure water (18.2 MΩ). Ten ions such as SO₄²⁻,
165 NO₃⁻, Cl⁻, NH₄⁺, and K⁺ were determined using ion chromatography (Dionex, ICS-
166 1100). A DRI model 2001 thermal-optical carbon analyzer was used to measure the
167 organic carbon (OC) and element carbon (EC) in each PM_{2.5} filter samples, of which
168 water-soluble organic carbon (WSOC) was extracted into Mill-Q pure water (18.2
169 MΩ) and ultimately quantified by a total organic carbon (TOC) analyzer (Model
170 TOC-L CPH, Shimadzu, Japan).



171 **2.3 Aerosol liquid water content (ALWC) and in situ pH**

172 The thermodynamic model (ISORROPIA-II) can provide robust predictions of the
173 aerosol liquid water content (ALWC) and in situ pH in PM_{2.5} samples. By combining
174 the actual temperature (T) and relative humidity (RH) in the atmosphere and the
175 composition, the ALWC and H⁺ loads can be simulated, which are used for
176 calculating the situ pH.

177 **2.4 Positive matrix factorization (PMF) source apportionment**

178 As a receptor model, PMF is a mathematical approach to quantify the contribution
179 of sources to samples, and has been widely used in the source apportionment of air
180 pollutant. More details of model can be found on the EPA website
181 ([https://www.epa.gov/air-research/epa-positive-matrix-factorization-50-fundamentals-](https://www.epa.gov/air-research/epa-positive-matrix-factorization-50-fundamentals-and-user-guide)
182 [and-user-guide](https://www.epa.gov/air-research/epa-positive-matrix-factorization-50-fundamentals-and-user-guide)). In this work, the organic matter (OM), EC WSOC, secondary
183 inorganic ions, biogenic SOA of all the samples served as the fingerprint species to
184 identify potential sources of the BSOA at Mt. Hua. After numerous tests, the model
185 would output an optimal solution according to the minor difference between Q_{True} and
186 Q_{Robust}; This is indicative of the robust model performance, as confirmed by the high
187 correlation coefficients between input and estimated values. Furthermore, as revealed
188 in our pervious study (Wu et al., 2022), the change of the main emission sources was
189 insignificant in air mass lifting process on Mt. Hua. Thus, the samples from both sites
190 were added together as one data matrix. Based on the Q values and interpretability,
191 five factors were obtained as the optimal solution after numerous testes, and the input
192 species matched well with simulated ones with significant correlations ($R^2 > 0.92$).



193 **3.1 Overview of OM during the campaign**

194 The bulk chemical compositions of PM_{2.5} during the campaign have been reported
195 in our previous work (Wu et al., 2022), and strongly substantiate that organic matter
196 (OM) is the principal component of PM_{2.5} at the surface and high elevation, with a
197 mass fraction of 32%~46%. For a deeper insight into the relative abundances, vertical
198 variability and sources of OM among two sampling sites, a comprehensive
199 comparison was given in Figure 1. The OM concentration was 30.0±10.4 µg/m³ at
200 MF site, approximately three-fold of that at MS site. Such abundant OM at surface
201 was apparently driven by fresh emissions from nearby roads and residences, as
202 evidenced by its strong correlation with hopanes (Figure S1(a), R²=0.46, *p*<0.05)
203 being a known tracer for combustion sources; Whereas, a weak correlation between
204 OM and hopanes was found at MF site, indicating the different sources for the OM
205 aloft. Moreover, subaerial OM was characterized by a higher nocturnal load, and
206 exhibited a decreased trend before midafternoon, which was thermally driven
207 boundary layer growth. Nonetheless, an inverse diel pattern was observed at high
208 elevation site with a daily OM peak at the moment (12:00~16:00) of strong
209 photochemical activity, suggesting that OM components aloft was probably driven by
210 photochemistry.

211 To determine the sources of OM at both sites, we performed a positive matrix
212 factorization (PMF) analysis, and identified five types of sources for OM (Figure S2).
213 Among these sources, biomass burning (BB) and fossil fuel combustion were believed
214 to the primary sources for OM at MF site, accounting for 52% and ~18% of OM



(Figure 1c), respectively. This coincided with that in Xi'an (~ 43% for BB) and Lin Village (30%~40% for BB) located on Guanzhong plain (Elser et al., 2016; Li et al., 2022). Whereas, merely ~24% of OM was explained by above anthropogenic sources at MS site; and most of OM aloft was dominated by biogenic secondary organic aerosol (BSOA, Figure 1d), with a fractional contribution of ~43% being septuple of that for subaerial OM. This elucidated a significant influence of biogenic primary and secondary sources on OM aloft.

3.2 Abundance and spatiotemporal variations of BSOA tracers

To characterize the spatiotemporal variations of biogenic SOA among two sites, a plenty of BSOA tracers including isoprene, monoterpene and sesquiterpene were quantified as summarized in Table1. The sum of detected BSOA tracers ranged 31 ng/m³ to 459 ng/m³ at MF site (269.4±1107.6 ng/m³, Figure S3), which was slightly lower than that at MS site (276.5±159.0 ng/m³); Such spatial pattern was also observed at Mt. Tai on North Chian Plain (Yi et al., 2021), further underscoring the significance of biogenic sources in mountainous OM formation aloft. Specifically, isoprene SOA tracers (BSOA_I) as the dominant species accounted for ~70% of the identified BSOA tracers, with average of 197.3±126.8 ng/m³ at MS site and 182.5±81.0 ng/m³ at MF site, respectively; These were comparable to that in the Kathmandu Valley of India (182.5±81.0 ng/m³) (Wan et al., 2019) and a mid-latitudinal forest zone (~240 ng/m³) (Zhu et al., 2016), but ~2 orders of magnitude higher than those measured over the North Pacific (3.6 ng/m³) (Fu et al., 2011). As for total monoterpene SOA tracers (BSOA_M) and sesquiterpene tracers (BSOA_S), their



237 abundances were lower by a factor of approximately 4~6 than BSOA_I, probably due
238 to a less emissions of monoterpene and sesquiterpene from the vegetation in this
239 region. Noteworthy, BSOA_M exhibited a converse spatial pattern, with a high load at
240 surface (MF: 52.4±23.1 ng/m³ vs. MS: 32.3±19.9 ng/m³). The coniferous plants, as
241 primary emitter of monoterpene (Gagan et al., 2023), may be less densely distributed
242 at the ground level relative to that on Mt. Hua; Thus, relatively abundant BSOA_M at
243 MF site likely affect by intensive BB activities that can also release numerous
244 monoterpenes, thereby potentially augmenting the surface BSOA_M levels. This can be
245 manifested by that BSOA_M strongly correlated with levoglucosan being known as BB
246 tracer, but weakly with C₂₉-alkane that mainly derived from vegetation emissions
247 (Figure S4).

248 **3.2.1 Isoprene SOA tracers**

249 A total of eight isoprene tracers formed by oxidated reactions of isoprene with NO_x
250 and OH₂[·] were identified in this study, namely C₅-alkene triols (cis-2-MTB, trans-2-
251 MTB and 3-MTB), 2-MGA, 2-methyltetrols (2-MT and 2-ME) and 3-MeTHF-3,4-
252 diols (trans-3-Methyltetrahydrofuran-3,4-diol and cis-3-Methyltetrahydrofuran-3,4-
253 diol). The BSOA_I at MF site exhibited a pronounced diurnal cycle, characterized by a
254 higher daytime load with an afternoon peak of 210.4±96.0 ng/m³ (Figure 2(a)). This
255 pattern aligns with temperature-driven characteristic of isoprene emission; and a
256 positive correlation between BSOA_I and temperature (R²=0.63) implied that a
257 substantial part of surface BSOA_I was expected to be formed locally (Figure S5 (a)),
258 given the short atmospheric lifetime of isoprene. Whereas, BSOA_I aloft was



259 characterized by an inverse diurnal variation, with a moderate enhancement in the
260 nocturnal load. As revealed by a high-elevation CWT analysis of BSOA_I (Figure 3),
261 relatively high nocturnal loading distributed over Mt. Hua and adjacent regions,
262 indicating that these SOA tracers aloft were significantly influenced by
263 regional/super-regional transport, especially during the nighttime.

264 2-methyltetrols (2-MTLs), as the predominant species at both sites, was more
265 abundant at high-elevation site ($98.6 \pm 68.5 \text{ ng/m}^3$) relative to surface site (73.8 ± 32.1
266 ng/m^3). This pattern was akin to the level observed at Mt. Tai (98 ng/m^3) (Yi et al.,
267 2021) and Mt. Changbai ($22 \sim 282 \text{ ng/m}^3$) (Wang et al., 2008). As the oxidation
268 products of isoprene under low/free-NO_x condition, 2-MTLs at MF site was
269 significantly formed during the daytime, and peaked at 12:00~16:00 LT (local time,
270 85.2 ng/m^3 , Figure 2(b)), corresponding to the period of reduced NO_x loads, high
271 temperature and intense solar radiation. Conversely, the concentration of 2-MTLs
272 aloft decreased progressively during the daytime, bottoming out until 16:00~20:00 LT;
273 This inverse diurnal pattern was probably due to the influx of the surface NO_x that
274 was transported aloft by the prevailing valley breeze, which subsequently inhibited
275 the 2-MTLs formation at MS site. Meanwhile, such relatively abundant NO_x
276 condition during the daytime would promote the formation of 2-MGA aloft
277 (culminating at 12:00~16:00 LT), as corroborated by a positive correlation between 2-
278 MGA and NO₂ (Figure S5 (c)). This finding was consistent with the laboratory
279 measurements of 2-MGA being derived from oxidization of isoprene with high NO_x
280 load (Wang et al., 2008). Moreover, surface 2-MGA also exhibited a similar diurnal



281 pattern with average of 28.6 ± 14.7 ng/m³ being 1.8-fold of that aloft, albeit a weak
282 relationship between 2-MGA and NO₂; This appreciably suggested that, beyond NO_x,
283 other factors also drove the 2-MGA formation at MF site.

284 C₅-alkene triols and 3-MeTHF-3,4-diols were another prevalent isoprene tracers, of
285 which concentration were comparable among two sites (Table 1). As the
286 photooxidation products under low/free-NO_x level, above two tracers exhibited a
287 diurnal cycle paralleled to that of 2-MTLs at two sites, and were characterized by
288 higher loads during nighttime. Despite that, the correlation between C₅-alkene triols
289 and 3-MeTHF-3,4-diols ($R^2 > 0.74$) was more robust than that involving 2-MTLs. This
290 was probably owing to that C₅-alkene triols and 3-MeTHF-3,4-diols were mainly
291 formed via acid-catalyzed intermolecular rearrangement reactions of epoxy-diols,
292 whereas 2-MTLs are likely to the result from nucleophilic addition of water to the
293 ring opening of epoxy-diols.

294 **3.2.2 Monoterpene SOA tracers**

295 The detected monoterpene tracers, including pinic acid (PA), cis-pinonic acid
296 (PNA), 3-hydroxyglutaric acid (3-HGA) and 3-methyl-1,2,3-butanetricarboxylic acid
297 (MBTCA), are mainly derived from photooxidation of α/β pinene initiated by $\cdot\text{OH}$
298 and O₃; Therefore, those four tracers exhibited a similar diurnal pattern, peaking at
299 12:00~16:00 LT when $\cdot\text{OH}$ and O₃ concentrations remained at highest daily level.
300 Based on the chamber measurements, PA and PNA are the early-generation products
301 of α/β pinene (Liu et al., 2022; Jaoui et al., 2005), merely accounting for ~10% and
302 ~12%-17% of the BSOA_M, respectively. Strikingly, PNA at two sampling sites was



303 more abundant by a factor of ~ 1.5 than PA, consistent with the observations at Mt. Tai,
304 Mt. Huang and in Duke Forest, North Carolina (Wang et al., 2023; Bhat and Fraser,
305 2007; Yi et al., 2021). The saturation vapor pressure of PNA is $\sim 7.2 \times 10^{-5}$ Pa (at 298
306 K, estimated by E-AIM model) is lower than that of PA ($\sim 2.0 \times 10^{-4}$ Pa), thus, PNA
307 can be readily nucleated and saturated in the atmosphere. Given that, PNA was
308 expected to have a higher abundance in aerosol than PA.

309 During the campaign, MBTCA was the most abundant BSOA_M tracer, explaining
310 more than half of the surface BSOA_M tracers at both sites, and followed by 3-HGA
311 with fractional contributions of $\sim 20\%$ to total BSOA_M. MBTCA and 3-HGA are
312 regarded as the later-generation products of α/β -pinene, and can be derived from
313 further photodegradation of PNA or PA; Thus, MBTCA/(PA+PNA) ratio (abbreviated
314 as M/P hereafter) is commonly used to estimate the α/β -pinene-derived SOA aging, of
315 which a higher value is indicative of more aged α/β -pinene SOA. As depicted in
316 Figure S6, the M/P value (2.6 ± 1.3) at MS site was ~ 1.4 -fold of that at MF site,
317 reflecting that the BSOA_M tracers aloft were more aged compare to that at surface;
318 This finding was coincided with the variation of oxidation state of carbon (OSc)
319 measured by the aerosol mass spectrometer. Additionally, a clear diurnal pattern of
320 M/P ratio was found at MF site, with a daily peak at 16:00~20:00 lagged that of
321 MBTCA by ~ 4 hr. However, the diurnal cycle of M/P ratio at MS site exhibited a
322 bimodal pattern, with two nearly equivalent peaks during the daytime (16:00~20:00)
323 and nighttime (4:00~8:00). Relatively high M/P ratios during nighttime indicated a
324 more aged state of nocturnal α/β -pinene SOA at upper atmosphere, markedly differing



325 from the ground-based observations. This was partially due to that the nocturnal
326 pollutants at MS site were mostly driven by regional or long-range transport (Figure
327 3), in which α/β -pinene SOA aloft would undergo a deeper aging, and leading to the
328 high M/P ratio.

329 **3.2.3 Sesquiterpene SOA tracers**

330 As a typical and abundant sesquiterpene, β -caryophyllene has been widely studied
331 due to its high reactivity and significant aerosol formation potential; and it can be
332 oxidated into β -caryophyllinic acid for via ozonolysis/photooxidation. In this study, β -
333 caryophyllinic acid was found to exhibit a relatively high concentration among the
334 detected BSOA tracers (Table 1), with average of 34.5 ± 19.1 ng/m³ at MF site and
335 56.0 ± 41.0 ng/m³ at MS site, respectively; These loads were comparative to Mt. Wuyi
336 ($7.6\text{--}54$ ng/m³) (Ren et al., 2019) and Mt. Tai ($0.05\text{--}48$ ng/m³) (Fu et al., 2012). As
337 expected, β -caryophyllinic acid robustly correlated with BSOA_M ($R^2 > 0.60$, $p < 0.05$) at
338 both sampling sites, indicating similar formation pathways for these species.
339 Additionally, the significant relationship between β -caryophyllinic acid and
340 levoglucosan at MF site could be a result of intensive biomass burning as indicated in
341 section 3.1; This observation aligns with previous findings that sesquiterpenes
342 accumulated in leaves and wood can be released in the biomass burning process,
343 subsequently oxidized to form β -caryophyllinic acid (Zhang et al., 2019b). Notably, β -
344 caryophyllene SOA tracers aloft in this study showed clearly enhanced concentrations
345 during the daytime from 10:00 to 16:00; whereas, the diurnal cycle of β -
346 caryophyllinic acid at MF site was less pronounced, despite significant diurnal



347 differences in Ox load and temperature that are known to influence heterogeneous
348 reactions of β -caryophyllene.

349 **3.3 Influencing factors of BSOA formation in upper troposphere**

350 A comparison of diurnal cycles of mass fraction of BSOA to OM ($F_{\text{BSOA/OM}}$) among
351 both sampling sites is illustrated in Figure 4. At MF site, a spike in $F_{\text{BSOA/OM}}$ was
352 observed at around 12:00-16:00 (Figure 4(a)), demonstrating that the surface BSOA
353 formation was strongly enhanced in the presence of abundant O_3/OH radical load and
354 high biogenic emissions, especially for isoprene SOA; Such diurnal variation was in
355 good agreement with the measurements at other sites (Zhang et al., 2019b; Zhu et al.,
356 2016; Lee et al., 2016). Whereas, $F_{\text{BSOA/OM}}$ for isoprene aloft exhibited a decreasing
357 pattern during photochemically active period (Figure 4(b)), reaching a minimum at
358 12:00-16:00. Although oxidant levels remained relatively high at this time, the
359 $F_{\text{BSOA/OM}}$ -isoprene was only 75% of that for the prior moment. Our previous
360 observational evidences have corroborated that surface-level anthropogenic pollutants
361 can be transported to upper atmosphere by the prevailing valley breeze (Wu et al.,
362 2022; Wu et al., 2024). Those anthropogenic pollutants (e.g., SO_2 , NO_x) likely
363 modulated BSOA formation aloft, leading to above unusual diurnal cycles $F_{\text{BSOA/OM}}$ -
364 isoprene. To elucidate the above hypothesis, the mantel test and random forest
365 analysis were applied for daytime BSOA aloft.

366 **3.3.1 Effects of meteorological factors on BSOA**

367 As shown in Figure 6(a), the BOSA positively correlated with ambient temperature
368 for daytime samples aloft, consistent with the temperature-dependent characteristic of



369 isoprene and monoterpene emissions from terrestrial vegetation; Thus, the relatively
370 high temperature was expected to enhance biogenic SOA yields from the
371 photooxidation of isoprene and monoterpenes, which also found at other mountainous
372 studies, e.g., Mt. Tai, Mt. Huang and Mt. Wuyi (Ren et al., 2019; Wang et al., 2023; Yi
373 et al., 2021). Additionally, the strong temperature-dependence of BSOA also indicated
374 a significant part of BSOA tracers aloft undergo rapid in-situ formation once the
375 oxidants concentrations built up during the daytime, contrasting with those during
376 nighttime. An insignificant correlation was observed between relative humidity and
377 BSOA tracers. However, the moist weather frequently occurred at MS site, even at the
378 daytime with average RH of $62.3 \pm 19.0\%$ (Wu et al., 2022); Thus, the less pronounced
379 variation can explain the insensitivity of BSOA formation to RH. Even so, the high
380 RH during daytime could indirectly influence BSOA formation aloft by modulating
381 aerosol water content (ALWC), aerosol acidity, gas–particle partitioning of BSOA
382 precursors.

383 **3.3.2 Effects of anthropogenic pollutants on BSOA**

384 Evidences from field and modeling studies indicates that biogenic SOA yield is
385 enhanced in presence of elevated NO_x level (Xu et al., 2015; Shrivastava et al., 2017).
386 However, the BSOA tracers aloft, especially isoprene-derived SOA, negatively
387 correlated with NO₂ ($r=0.36$, $P<0.05$) (Figure 6(a)). Additionally, the 2-MTLs/2-MGA
388 ratio, which is indicative of NO_x influence on SOA formation, followed a similar
389 diurnal pattern to that of the $F_{\text{BSOA}/\text{OM-isoprene}}$ (Figure 6(b)). All those findings indicated
390 that the NO₂ transported from the surface to high altitude may limit the formation of



391 SOA_I in the daytime. As is well known, isoprene oxidization primarily follows two
392 pathways, i.e., HO₂ pathway forming 2-MTLs in NO_x-limited conditions and
393 NO/NO₂ channel yielding 2-MGA in high-NO_x scenarios. Thereby, we hypothesized
394 that the increasing NO_x at MS site may perturb BSOA formation by competing with
395 HO₂ pathway, diminishing the net SOA yield relative to NO_x-limited conditions. This
396 was consistent with experimental finding conducted by Thornton et al. (2020), who
397 demonstrated that a nonlinear dependence of BSOA yield on NO_x level and a steep
398 decrease in isoprene-derived SOA formation beyond a certain NO_x threshold; Notably,
399 they also found that, at high NO_x level (NO~500 ppt) that is akin to our daytime
400 observations at MS site, the maximum BSOA yield is 10% lower than that at low
401 NO_x.

402 As shown in Figure 5(c), the sulfate presented a statistically significant positive
403 relationship with BSOA_I. This feature appeared to be common for other similar filed
404 studies (Wang et al., 2008; Xu et al., 2015; Liu et al., 2017), underscoring the
405 significant role of sulfate in the isoprene-derived SOA formation. According to
406 laboratory studies (Eddingsaas et al., 2010), the sulfate can act as nucleophiles to
407 facilitate the ring-opening reaction of epoxydiols (IEPOX), which is pivotal oxidation
408 product of isoprene when organic peroxy radicals mainly react with HO₂ radicals.
409 While, the sulfate level was moderately enhanced, with a daily maximum at 12:00-
410 16:00 LT (Figure 5(c)); This is indicative of the further formation in air mass lifting
411 process (Wu et al., 2022). An increase in sulfate would boost the ion strength and
412 salting-in effect of aerosol, thereby enhancing IEPOX reactive uptake and inhibiting



413 its reversible partitioning back to the gas phase. Furthermore, sulfate can modulate the
414 H^+ level, acting as a more efficient proton donor to catalyze IEPOX ring opening and
415 isoprene ozonolysis; Thus, H^+ concentration predicted by thermodynamic model
416 ISORROPIA II positively correlates with $BSOA_I$, as indicated in Figure 5(a).

417 Additionally, the further formation of sulfate in lifting air mass can also promote an
418 enhancement in ALWC aloft (Figure 5(c)), with a daytime maximum at 12:00-16:00
419 LT, which temporally coincided with a significant decrease in $F_{BSOA-isoprene/OM}$. This
420 pattern suggested an inhibited effect of aerosol water on BSOA formation, consistent
421 with laboratory observation by Gaston et al. (2014), who found a 50% reduction in
422 IEPOX reactive uptake on NH_4HSO_4 particles as RH increases from 30% to 70%. As
423 evidenced by previous studies (Xu et al., 2015; Riedel et al., 2015), the abundant
424 aerosol water can moderate BSOA formation by affecting ionic strength, proton
425 donor/nucleophilic activity, and consequently altering the reactive uptake (e.g.,
426 IEPOX) and subsequent reactions. To quantitatively evaluate the effects of ALWC,
427 the pseudo-first-order heterogeneous reaction rate constant for IEPOX reactive uptake
428 (k_{het}) was calculated for the samples at MS site following the method of Gaston et al.
429 (2014) (Text S1). The simulated uptake coefficient of IEPOX (γ_{IEPOX}) during the
430 daytime was 4.3×10^{-4} being in the range of field and laboratory observations ($0.1 -$
431 6.5×10^{-4}) (Zhang et al., 2017; Gaston et al., 2014). As shown in Figure 6, the high
432 ALWC commonly corresponds to low γ_{IEPOX} during the daytime, characterized by
433 weak ionic strength and low $H_{(aq)}^+$ concentration. This indicates that enhanced ALWC
434 at MS likely impeded the IEPOX uptake onto particle surface. Consequently, the



435 average k_{het} at 12:00-16:00 L was merely 9.8×10^{-8} 1/s, which was an order of
436 magnitude lower than that in the rest of daytime. These results underscore that
437 enhanced ALWC during the daytime would lead to an insufficiently rapid
438 heterogeneous reaction of IEPOX, and finally diminished the BSOA_I formation.

439 To elucidate the key factors that affect BSOA formation aloft, a RF analysis was
440 conducted for the daytime samples at MS site. The RF model commendably
441 highlighted the significance of the factors contributing to BSOA_I formation, as
442 evidenced by the robust correlations between the predicted and observed data for both
443 the training and testing datasets ($R^2 > 0.8$, Table S1), along with minimal error metrics.
444 As shown in Figure 5(d), the daytime BSOA_I concentration was largely affected by
445 the ozone (~29%), with a robust positive correlation between them (Figure 5(a)); This
446 indicated that enhanced O₃ is likely to augment isoprene oxidation products aloft.
447 Additionally, NO₂ and ALWC also play pivotal roles in BSOA_I formation, with the
448 importance of ~19% and 13.3%, respectively; These findings further corroborated that
449 the enhanced NO_x may lead an impedimental effect on the daytime BSOA formation
450 in the upper boundary layer of Mt. Hua. Such limiting effect on isoprene-derived SOA
451 formation under high NO_x scenario was also found in Eastern China and Amazon
452 (Zhang et al., 2017; De Sa et al., 2017).

453 **4 Summary and conclusion**

454 The PM_{2.5} samples with 4 h intervals were synchronously collected at mountain
455 foot and mountainside of Mt. Hua, to elucidate the chemical evolution and
456 spatiotemporal differences of the organic matter among two sites. At the MF site, the



457 anthropogenic emissions, such as biomass burning and fossil fuel combustion, were
458 identified as substantial contributors to the OM, accounting for more than 70% of
459 total OM. Whereas, only ~24% of OM aloft was derived from anthropogenic
460 emissions, with biogenic secondary organic aerosol (43%) emerging as the
461 predominant OM source aloft.

462 Three distinct types of BSOA tracers were identified, predominantly featuring
463 isoprene-derived species. At MF site, most of the BSOA tracers were more abundant
464 during the daytime and peaked at 12:00~16:00 LT, indicative of photochemical
465 oxidation as the primary formation pathway. Whereas, there is a marked decrease in
466 the absolute concentration and relative abundance of daytime isoprene-derived tracers
467 in the upper atmosphere. This decline can be attributed to the intrusion of ground-
468 level NO_x, which significantly modifies BSOA_I formation at higher altitudes by
469 inhibiting the HO₂· oxidative pathway. Additionally, a further formation of sulfate in
470 lifting air mass moderately enhanced ALWC aloft, leading to a low IEPOX reactive
471 uptake on the particle surface, which would also limit the daytime BSOA_I formation
472 aloft. Unfortunately, our limited data does not allow us to peer into the fundamental
473 mechanistic and kinetic details of this process. All these findings highlighted the
474 complex and regional variability of the influences of NO_x on BSOA formation. Over
475 the past decade, atmospheric environment in China has undergone substantial change
476 unevenly implemented emission controls, resulting in much higher levels of NO₂
477 compared with SO₂ (Zheng et al., 2018). These alterations in pollutant emissions
478 could substantially affect BSOA formation; Thus, there is an urgent need for long-



term characterization of BSOA to better assess its potential impacts on radiative forcing, human health, and to fully understand the anthropogenic–biogenic interactions.

Data availability. The data used in this study are freely available at <https://doi.org/10.5281/zenodo.15164940> (Wu, 2025). And Meteorological data and hourly PM_{2.5}, NO₂, O₃ concentrations can be obtained from <https://doi.org/10.5281/zenodo.7413640> (Wu, 2022).

Author contributions. G.W. designed research and contributed analytic tools. C.W., C.C. and J.L. collected the samples. C.W. and Y.C. conducted the sample analysis. C.W. and G.W. performed the data interpretation. C.W. wrote the paper. All authors contributed to the paper with useful scientific discussions.

Competing interests. The authors declare no competing interest.

Acknowledgements. This work was financially supported by the National Natural Science Foundation of China (grant no. 42477097, 42130704) and the National Key Research and Development Program of China (grant no. 2023YFC3707401).

References

- Bhat, S. and Fraser, M. P.: Primary source attribution and analysis of α -pinene photooxidation products in Duke Forest, North Carolina, *Atmospheric Environment*, 41, 2958–2966, 10.1016/j.atmosenv.2006.12.018, 2007.
- Coggon, M. M., Gkatzelis, G. I., McDonald, B. C., Gilman, J. B., Schwantes, R. H., Abuhassan, N., Aikin, K. C., Arend, M. F., Berkoff, T. A., Brown, S. S., Campos, T. L., Dickerson, R. R., Gronoff, G., Hurley, J. F., Isaacman-VanWertz, G., Koss, A. R., Li, M., McKeen, S. A., Moshary, F., Peischl, J., Pospisilova, V., Ren, X., Wilson, A., Wu, Y., Trainer, M., and Warneke, C.: Volatile chemical product emissions enhance ozone and modulate urban chemistry, *Proceedings of the National Academy of Sciences of the United States of America*, 118, 10.1073/pnas.2026653118, 2021.
- de Sa, S. S., Palm, B. B., Campuzano-Jost, P., Day, D. A., Newburn, M. K., Hu, W., Isaacman-VanWertz, G., Yee, L. D., Thalman, R., Brito, J., Carbone, S., Artaxo, P., Goldstein, A. H., Manzi, A. O., Souza, R. A. F., Mei, F., Shilling, J. E., Springston, S. R., Wang, J., Surratt, J. D., Alexander,



- 508 M. L., Jimenez, J. L., and Martin, S. T.: Influence of urban pollution on the production of organic
509 particulate matter from isoprene epoxydiols in central Amazonia, *Atmospheric Chemistry and*
510 *Physics*, 17, 6611-6629, 10.5194/acp-17-6611-2017, 2017.
- 511 Dong, X., Liu, Y., Li, X., Yue, M., Liu, Y., Ma, Z., Zheng, H., Huang, R., and Wang, M.: Modeling
512 Analysis of Biogenic Secondary Organic Aerosol Dependence on Anthropogenic Emissions in
513 China, *Environmental Science & Technology Letters*, 9, 286-292, 10.1021/acs.estlett.2c00104,
514 2022.
- 515 Eddingsaas, N. C., VanderVelde, D. G., and Wennberg, P. O.: Kinetics and Products of the Acid-
516 Catalyzed Ring-Opening of Atmospherically Relevant Butyl Epoxy Alcohols, *Journal of Physical*
517 *Chemistry A*, 114, 8106-8113, 10.1021/jp103907c, 2010.
- 518 Elser, M., Huang, R.-J., Wolf, R., Slowik, J. G., Wang, Q., Canonaco, F., Li, G., Bozzetti, C.,
519 Daellenbach, K. R., Huang, Y., Zhang, R., Li, Z., Cao, J., Baltensperger, U., El-Haddad, I., and
520 Prevot, A. S. H.: New insights into PM_{2.5} chemical composition and sources in two major cities in
521 China during extreme haze events using aerosol mass spectrometry, *Atmospheric Chemistry and*
522 *Physics*, 16, 3207-3225, 10.5194/acp-16-3207-2016, 2016.
- 523 Fu, P., Kawamura, K., and Miura, K.: Molecular characterization of marine organic aerosols collected
524 during a round-the-world cruise, *Journal of Geophysical Research-Atmospheres*, 116,
525 10.1029/2011jd015604, 2011.
- 526 Fu, P., Kawamura, K., Chen, J., and Miyazaki, Y.: Secondary Production of Organic Aerosols from
527 Biogenic VOCs over Mt. Fuji, Japan, *Environmental Science & Technology*, 48, 8491-8497,
528 10.1021/es500794d, 2014.
- 529 Fu, P. Q., Kawamura, K., Chen, J., Li, J., Sun, Y. L., Liu, Y., Tachibana, E., Aggarwal, S. G., Okuzawa,
530 K., Tanimoto, H., Kanaya, Y., and Wang, Z. F.: Diurnal variations of organic molecular tracers and
531 stable carbon isotopic composition in atmospheric aerosols over Mt. Tai in the North China Plain:
532 an influence of biomass burning, *Atmospheric Chemistry and Physics*, 12, 8359-8375,
533 10.5194/acp-12-8359-2012, 2012.
- 534 Gagan, S., Sarang, K., Rudzinski, K. J., Liu, R., Szmigielski, R., and Zhang, Y.: Synthetic strategies for
535 oxidation products from biogenic volatile organic compounds in the atmosphere: A review,
536 *Atmospheric Environment*, 312, 10.1016/j.atmosenv.2023.120017, 2023.
- 537 Gaston, C. J., Riedel, T. P., Zhang, Z., Gold, A., Surratt, J. D., and Thornton, J. A.: Reactive Uptake of
538 an Isoprene-Derived Epoxydiol to Submicron Aerosol Particles, *Environmental Science &*
539 *Technology*, 48, 11178-11186, 10.1021/es5034266, 2014.
- 540 Guenther, A. B., Jiang, X., Heald, C. L., Sakulyanontvittaya, T., Duhl, T., Emmons, L. K., and Wang,
541 X.: The Model of Emissions of Gases and Aerosols from Nature version 2.1 (MEGAN2.1): an
542 extended and updated framework for modeling biogenic emissions, *Geoscientific Model*
543 *Development*, 5, 1471-1492, 10.5194/gmd-5-1471-2012, 2012.
- 544 Hallquist, M., Wenger, J. C., Baltensperger, U., Rudich, Y., Simpson, D., Claeys, M., Dommen, J.,
545 Donahue, N. M., George, C., Goldstein, A. H., Hamilton, J. F., Herrmann, H., Hoffmann, T.,
546 Iinuma, Y., Jang, M., Jenkin, M. E., Jimenez, J. L., Kiendler-Scharr, A., Maenhaut, W., McFiggans,
547 G., Mentel, T. F., Monod, A., Prevot, A. S. H., Seinfeld, J. H., Surratt, J. D., Szmigielski, R., and
548 Wildt, J.: The formation, properties and impact of secondary organic aerosol: current and
549 emerging issues, *Atmospheric Chemistry and Physics*, 9, 5155-5236, 10.5194/acp-9-5155-2009,
550 2009.
- 551 Hodnebrog, O., Myhre, G., and Samset, B. H.: How shorter black carbon lifetime alters its climate



- effect, *Nature Communications*, 5, 10.1038/ncomms6065, 2014.
- Hodzic, A., Kasibhatla, P. S., Jo, D. S., Cappa, C. D., Jimenez, J. L., Madronich, S., and Park, R. J.: Rethinking the global secondary organic aerosol (SOA) budget: stronger production, faster removal, shorter lifetime, *Atmospheric Chemistry and Physics*, 16, 7917-7941, 10.5194/acp-16-7917-2016, 2016.
- Jaoui, M., Kleindienst, T. E., Lewandowski, M., Offenberg, J. H., and Edney, E. O.: Identification and quantification of aerosol polar oxygenated compounds bearing carboxylic or hydroxyl groups. 2. Organic tracer compounds from monoterpenes, *Environmental Science & Technology*, 39, 5661-5673, 10.1021/es048111b, 2005.
- Kelly, J. M., Doherty, R. M., O'Connor, F. M., and Mann, G. W.: The impact of biogenic, anthropogenic, and biomass burning volatile organic compound emissions on regional and seasonal variations in secondary organic aerosol, *Atmospheric Chemistry and Physics*, 18, 7393-7422, 10.5194/acp-18-7393-2018, 2018.
- Lee, A. K. Y., Abbatt, J. P. D., Leaitch, W. R., Li, S.-M., Sjostedt, S. J., Wentzell, J. J. B., Liggio, J., and Macdonald, A. M.: Substantial secondary organic aerosol formation in a coniferous forest: observations of both day- and nighttime chemistry, *Atmospheric Chemistry and Physics*, 16, 6721-6733, 10.5194/acp-16-6721-2016, 2016.
- Li, J., Li, J., Wang, G., Ho, K. F., Han, J., Dai, W., Wu, C., Cao, C., and Liu, L.: In-vitro oxidative potential and inflammatory response of ambient PM_{2.5} in a rural region of Northwest China: Association with chemical compositions and source contribution, *Environmental Research*, 205, 10.1016/j.envres.2021.112466, 2022.
- Li, J. J., Wang, G. H., Cao, J. J., Wang, X. M., and Zhang, R. J.: Observation of biogenic secondary organic aerosols in the atmosphere of a mountain site in central China: temperature and relative humidity effects, *Atmospheric Chemistry and Physics*, 13, 11535-11549, 10.5194/acp-13-11535-2013, 2013.
- Lin, Y.-H., Zhang, H., Pye, H. O. T., Zhang, Z., Marth, W. J., Park, S., Arashiro, M., Cui, T., Budisulistiorini, H., Sexton, K. G., Vizuete, W., Xie, Y., Luecken, D. J., Piletic, I. R., Edney, E. O., Bartolotti, L. J., Gold, A., and Surratt, J. D.: Epoxide as a precursor to secondary organic aerosol formation from isoprene photooxidation in the presence of nitrogen oxides, *Proceedings of the National Academy of Sciences of the United States of America*, 110, 6718-6723, 10.1073/pnas.1221150110, 2013.
- Liu, J., Russell, L. M., Lee, A. K. Y., McKinney, K. A., Surratt, J. D., and Ziemann, P. J.: Observational evidence for pollution-influenced selective uptake contributing to biogenic secondary organic aerosols in the southeastern US, *Geophysical Research Letters*, 44, 8056-8064, 10.1002/2017gl074665, 2017.
- Liu, J., D'Ambro, E. L., Lee, B. H., Schobesberger, S., Bell, D. M., Zaveri, R. A., Zelenyuk, A., Thornton, J. A., and Shilling, J. E.: Monoterpene Photooxidation in a Continuous-Flow Chamber: SOA Yields and Impacts of Oxidants, NO_x, and VOC Precursors, *Environmental Science & Technology*, 56, 12066-12076, 10.1021/acs.est.2c02630, 2022.
- Marais, E. A., Jacob, D. J., Jimenez, J. L., Campuzano-Jost, P., Day, D. A., Hu, W., Krechmer, J., Zhu, L., Kim, P. S., Miller, C. C., Fisher, J. A., Travis, K., Yu, K., Hanisco, T. F., Wolfe, G. M., Arkinson, H. L., Pye, H. O. T., Froyd, K. D., Liao, J., and McNeill, V. F.: Aqueous-phase mechanism for secondary organic aerosol formation from isoprene: application to the southeast United States and co-benefit of SO₂ emission controls, *Atmospheric Chemistry and Physics*, 16,



- 1603-1618, 10.5194/acp-16-1603-2016, 2016.
- McFiggans, G., Mentel, T. F., Wildt, J., Pullinen, I., Kang, S., Kleist, E., Schmitt, S., Springer, M., Tillmann, R., Wu, C., Zhao, D., Hallquist, M., Faxon, C., Le Breton, M., Hallquist, A. M., Simpson, D., Bergstrom, R., Jenkin, M. E., Ehn, M., Thornton, J. A., Alfarra, M. R., Bannan, T. J., Percival, C. J., Priestley, M., Topping, D., and Kiendler-Scharr, A.: Secondary organic aerosol reduced by mixture of atmospheric vapours, *Nature*, 565, 587-593, 10.1038/s41586-018-0871-y, 2019.
- Mellouki, A., Wallington, T. J., and Chen, J.: Atmospheric Chemistry of Oxygenated Volatile Organic Compounds: Impacts on Air Quality and Climate, *Chemical Reviews*, 115, 3984-4014, 10.1021/cr500549n, 2015.
- Nazarenko, L., Rind, D., Tsigaridis, K., Del Genio, A. D., Kelley, M., and Tausnev, N.: Interactive nature of climate change and aerosol forcing, *Journal of Geophysical Research-Atmospheres*, 122, 3457-3480, 10.1002/2016jd025809, 2017.
- Ng, N. L., Brown, S. S., Archibald, A. T., Atlas, E., Cohen, R. C., Crowley, J. N., Day, D. A., Donahue, N. M., Fry, J. L., Fuchs, H., Griffin, R. J., Guzman, M. I., Herrmann, H., Hodzic, A., Iinuma, Y., Jimenez, J. L., Kiendler-Scharr, A., Lee, B. H., Luecken, D. J., Mao, J., McLaren, R., Mutzel, A., Osthoff, H. D., Ouyang, B., Picquet-Varraut, B., Platt, U., Pye, H. O. T., Rudich, Y., Schwantes, R. H., Shiraiwa, M., Stutz, J., Thornton, J. A., Tilgner, A., Williams, B. J., and Zaveri, R. A.: Nitrate radicals and biogenic volatile organic compounds: oxidation, mechanisms, and organic aerosol, *Atmospheric Chemistry and Physics*, 17, 2103-2162, 10.5194/acp-17-2103-2017, 2017.
- Offenberg, J. H., Lewandowski, M., Edney, E. O., Kleindienst, T. E., and Jaoui, M.: Influence of Aerosol Acidity on the Formation of Secondary Organic Aerosol from Biogenic Precursor Hydrocarbons, *Environmental Science & Technology*, 43, 7742-7747, 10.1021/es901538e, 2009.
- Pye, H. O. T., Chan, A. W. H., Barkley, M. P., and Seinfeld, J. H.: Global modeling of organic aerosol: the importance of reactive nitrogen (NO_x and NO₃), *Atmospheric Chemistry and Physics*, 10, 11261-11276, 10.5194/acp-10-11261-2010, 2010.
- Ren, Y., Wang, G., Tao, J., Zhang, Z., Wu, C., Wang, J., Li, J., Wei, J., Li, H., and Meng, F.: Seasonal characteristics of biogenic secondary organic aerosols at Mt. Wuyi in Southeastern China: Influence of anthropogenic pollutants, *Environmental Pollution*, 252, 493-500, 10.1016/j.envpol.2019.05.077, 2019.
- Ridley, D. A., Heald, C. L., Ridley, K. J., and Kroll, J. H.: Causes and consequences of decreasing atmospheric organic aerosol in the United States, *Proceedings of the National Academy of Sciences of the United States of America*, 115, 290-295, 10.1073/pnas.1700387115, 2018.
- Riedel, T. P., Lin, Y.-H., Budisulistiorini, H., Gaston, C. J., Thornton, J. A., Zhang, Z., Vizuete, W., Gold, A., and Surratt, J. D.: Heterogeneous Reactions of Isoprene-Derived Epoxides: Reaction Probabilities and Molar Secondary Organic Aerosol Yield Estimates, *Environmental Science & Technology Letters*, 2, 38-42, 10.1021/ez500406f, 2015.
- Scott, C. E., Rap, A., Spracklen, D. V., Forster, P. M., Carslaw, K. S., Mann, G. W., Pringle, K. J., Kivekas, N., Kulmala, M., Lihavainen, H., and Tunved, P.: The direct and indirect radiative effects of biogenic secondary organic aerosol, *Atmospheric Chemistry and Physics*, 14, 447-470, 10.5194/acp-14-447-2014, 2014.
- Shrivastava, M., Cappa, C. D., Fan, J., Goldstein, A. H., Guenther, A. B., Jimenez, J. L., Kuang, C., Laskin, A., Martin, S. T., Ng, N. L., Petaja, T., Pierce, J. R., Rasch, P. J., Roldin, P., Seinfeld, J. H., Shilling, J., Smith, J. N., Thornton, J. A., Volkamer, R., Wang, J., Worsnop, D. R., Zaveri, R. A.,



- 640 Zelenyuk, A., and Zhang, Q.: Recent advances in understanding secondary organic aerosol:
641 Implications for global climate forcing, *Reviews of Geophysics*, 55, 509-559,
642 10.1002/2016rg000540, 2017.
- 643 Thornton, J. A., Shilling, J. E., Shrivastava, M., D'Ambro, E. L., Zawadowicz, M. A., and Liu, J.: A
644 Near-Explicit Mechanistic Evaluation of Isoprene Photochemical Secondary Organic Aerosol
645 Formation and Evolution: Simulations of Multiple Chamber Experiments with and without Added
646 NO_x, *Acs Earth and Space Chemistry*, 4, 1161-1181, 10.1021/acsearthspacechem.0c00118, 2020.
- 647 Wan, X., Kang, S., Rupakheti, M., Zhang, Q., Tripathi, L., Guo, J., Chen, P., Rupakheti, D., Panday, A.
648 K., Lawrence, M. G., Kawamura, K., and Cong, Z.: Molecular characterization of organic aerosols
649 in the Kathmandu Valley, Nepal: insights into primary and secondary sources, *Atmospheric
650 Chemistry and Physics*, 19, 2725-2747, 10.5194/acp-19-2725-2019, 2019.
- 651 Wang, G., Zhang, S., Wu, C., Zhu, T., Xu, X., Ge, S., Sun, H., Sun, Z., Wang, J., Ji, Y., Gao, J., Ren, Y.,
652 Li, H., Zhang, F., Wang, Y., and Seinfeld, J. H.: Atmospheric sulfate aerosol formation enhanced
653 by interfacial anions, *Pnas Nexus*, 4, 10.1093/pnasnexus/pgaf058, 2025.
- 654 Wang, G., Zhang, R., Gomez, M. E., Yang, L., Zamora, M. L., Hu, M., Lin, Y., Peng, J., Guo, S., Meng,
655 J., Li, J., Cheng, C., Hu, T., Ren, Y., Wang, Y., Gao, J., Cao, J., An, Z., Zhou, W., Li, G., Wang, J.,
656 Tian, P., Marrero-Ortiz, W., Sequest, J., Du, Z., Zheng, J., Shang, D., Zeng, L., Shao, M., Wang, W.,
657 Huang, Y., Wang, Y., Zhu, Y., Li, Y., Hu, J., Pan, B., Cai, L., Cheng, Y., Ji, Y., Zhang, F., Rosenfeld,
658 D., Liss, P. S., Duce, R. A., Kolb, C. E., and Molina, M. J.: Persistent sulfate formation from
659 London Fog to Chinese haze, *Proceedings of the National Academy of Sciences of the United
660 States of America*, 113, 13630-13635, 10.1073/pnas.1616540113, 2016.
- 661 Wang, G. H. and Kawamura, K.: Molecular characteristics of urban organic aerosols from Nanjing: A
662 case study of a mega-city in China, *Environmental Science & Technology*, 39, 7430-7438,
663 10.1021/es051055+, 2005.
- 664 Wang, G. H., Li, J. J., Cheng, C. L., Zhou, B. H., Xie, M. J., Hu, S. Y., Meng, J. J., Sun, T., Ren, Y. Q.,
665 Cao, J. J., Liu, S. X., Zhang, T., and Zhao, Z. Z.: Observation of atmospheric aerosols at Mt. Hua
666 and Mt. Tai in central and east China during spring 2009-Part 2: Impact of dust storm on organic
667 aerosol composition and size distribution, *Atmospheric Chemistry and Physics*, 12, 4065-4080,
668 10.5194/acp-12-4065-2012, 2012.
- 669 Wang, W., Wu, M. H., Li, L., Zhang, T., Liu, X. D., Feng, J. L., Li, H. J., Wang, Y. J., Sheng, G. Y.,
670 Claeys, M., and Fu, J. M.: Polar organic tracers in PM_{2.5} aerosols from forests in eastern China,
671 *Atmospheric Chemistry and Physics*, 8, 7507-7518, 10.5194/acp-8-7507-2008, 2008.
- 672 Wang, Y., Meng, J., Huang, T., Ma, J., Wang, Y., Zhang, X., Guo, Q., Yang, J., and Hou, Z.: Contrasting
673 molecular characteristics and formation mechanisms of biogenic and anthropogenic secondary
674 organic aerosols at the summit and foot of Mt. Huang, East China, *Science of the Total
675 Environment*, 895, 10.1016/j.scitotenv.2023.165116, 2023.
- 676 Wu, C.: Synchronous observation of biogenic secondary organic aerosol at Mt. Hua, Zenodo [data set],
677 <https://doi.org/10.5281/zenodo.15164940>, 2025.
- 678 Wu, C.: Synchronous observation of aerosol at Mt. Hua, Version 1, Zenodo [data set],
679 <https://doi.org/10.5281/zenodo.7413640>, 2022.
- 680 Wu, C., Liu, X., Zhang, K., Zhang, S., Cao, C., Li, J., Li, R., Zhang, F., and Wang, G.: Measurement
681 report: Formation of tropospheric brown carbon in a lifting air mass, *Atmospheric Chemistry and
682 Physics*, 24, 9263-9275, 10.5194/acp-24-9263-2024, 2024.
- 683 Wu, C., Cao, C., Li, J., Lv, S., Li, J., Liu, X., Zhang, S., Liu, S., Zhang, F., Meng, J., and Wang, G.:



- 684 Different physicochemical behaviors of nitrate and ammonium during transport: a case study on
685 Mt. Hua, China, *Atmospheric Chemistry and Physics*, 22, 15621-15635, 10.5194/acp-22-15621-
686 2022, 2022.
- 687 Wu, K., Yang, X., Chen, D., Gu, S., Lu, Y., Jiang, Q., Wang, K., Ou, Y., Qian, Y., Shao, P., and Lu, S.:
688 Estimation of biogenic VOC emissions and their corresponding impact on ozone and secondary
689 organic aerosol formation in China, *Atmospheric Research*, 231, 10.1016/j.atmosres.2019.104656,
690 2020.
- 691 Xu, L., Middlebrook, A. M., Liao, J., de Gouw, J. A., Guo, H., Weber, R. J., Nenes, A., Lopez-Hilfiker,
692 F. D., Lee, B. H., Thornton, J. A., Brock, C. A., Neuman, J. A., Nowak, J. B., Pollack, I. B., Welti,
693 A., Graus, M., Warneke, C., and Ng, N. L.: Enhanced formation of isoprene-derived organic
694 aerosol in sulfur-rich power plant plumes during Southeast Nexus, *Journal of Geophysical*
695 *Research-Atmospheres*, 121, 11137-11153, 10.1002/2016jd025156, 2016.
- 696 Xu, L., Guo, H., Boyd, C. M., Klein, M., Bougiatioti, A., Cerully, K. M., Hite, J. R., Isaacman-
697 VanWertz, G., Kreisberg, N. M., Knote, C., Olson, K., Koss, A., Goldstein, A. H., Hering, S. V., de
698 Gouw, J., Baumann, K., Lee, S.-H., Nenes, A., Weber, R. J., and Ng, N. L.: Effects of
699 anthropogenic emissions on aerosol formation from isoprene and monoterpenes in the
700 southeastern United States, *Proceedings of the National Academy of Sciences of the United States*
701 *of America*, 112, 37-42, 10.1073/pnas.1417609112, 2015.
- 702 Yi, Y., Meng, J., Hou, Z., Wang, G., Zhou, R., Li, Z., Li, Y., Chen, M., Liu, X., Li, H., and Yan, L.:
703 Contrasting compositions and sources of organic aerosol markers in summertime PM_{2.5} from
704 urban and mountainous regions in the North China Plain, *Science of the Total Environment*, 766,
705 10.1016/j.scitotenv.2020.144187, 2021.
- 706 Zhang, H., Yee, L. D., Lee, B. H., Curtis, M. P., Worton, D. R., Isaacman-VanWertz, G., Offenberg, J.
707 H., Lewandowski, M., Kleindienst, T. E., Beaver, M. R., Holder, A. L., Lonneman, W. A.,
708 Docherty, K. S., Jaoui, M., Pye, H. O. T., Hu, W., Day, D. A., Campuzano-Jost, P., Jimenez, J. L.,
709 Guo, H., Weber, R. J., de Gouw, J., Koss, A. R., Edgerton, E. S., Brune, W., Mohr, C., Lopez-
710 Hilfiker, F. D., Lutz, A., Kreisberg, N. M., Spielman, S. R., Hering, S. V., Wilson, K. R., Thornton,
711 J. A., and Goldstein, A. H.: Monoterpenes are the largest source of summertime organic aerosol in
712 the southeastern United States, *Proceedings of the National Academy of Sciences of the United*
713 *States of America*, 115, 2038-2043, 10.1073/pnas.1717513115, 2018.
- 714 Zhang, Q., Zheng, Y., Tong, D., Shao, M., Wang, S., Zhang, Y., Xu, X., Wang, J., He, H., Liu, W., Ding,
715 Y., Lei, Y., Li, J., Wang, Z., Zhang, X., Wang, Y., Cheng, J., Liu, Y., Shi, Q., Yan, L., Geng, G.,
716 Hong, C., Li, M., Liu, F., Zheng, B., Cao, J., Ding, A., Gao, J., Fu, Q., Huo, J., Liu, B., Liu, Z.,
717 Yang, F., He, K., and Hao, J.: Drivers of improved PM_{2.5} air quality in China from 2013 to 2017,
718 *Proceedings of the National Academy of Sciences of the United States of America*, 116, 24463-
719 24469, 10.1073/pnas.1907956116, 2019a.
- 720 Zhang, Y.-Q., Chen, D.-H., Ding, X., Li, J., Zhang, T., Wang, J.-Q., Cheng, Q., Jiang, H., Song, W., Ou,
721 Y.-B., Ye, P.-L., Zhang, G., and Wang, X.-M.: Impact of anthropogenic emissions on biogenic
722 secondary organic aerosol: observation in the Pearl River Delta, southern China, *Atmospheric*
723 *Chemistry and Physics*, 19, 14403-14415, 10.5194/acp-19-14403-2019, 2019b.
- 724 Zhang, Y., Tang, L., Sun, Y., Favez, O., Canonaco, F., Albinet, A., Couvidat, F., Liu, D., Jayne, J. T.,
725 Wang, Z., Croteau, P. L., Canagaratna, M. R., Zhou, H.-c., Prevot, A. S. H., and Worsnop, D. R.:
726 Limited formation of isoprene epoxydiols-derived secondary organic aerosol under NO_x-rich
727 environments in Eastern China, *Geophysical Research Letters*, 44, 2035-2043,



728 10.1002/2016gl072368, 2017.
729 Zheng, B., Tong, D., Li, M., Liu, F., Hong, C., Geng, G., Li, H., Li, X., Peng, L., Qi, J., Yan, L., Zhang,
730 Y., Zhao, H., Zheng, Y., He, K., and Zhang, Q.: Trends in China's anthropogenic emissions since
731 2010 as the consequence of clean air actions, *Atmospheric Chemistry and Physics*, 18, 14095-
732 14111, 10.5194/acp-18-14095-2018, 2018.
733 Zheng, Y., Horowitz, L. W. W., Menzel, R., Paynter, D. J., Naik, V., Li, J., and Mao, J.: Anthropogenic
734 amplification of biogenic secondary organic aerosol production, *Atmospheric Chemistry and*
735 *Physics*, 23, 8993-9007, 10.5194/acp-23-8993-2023, 2023.
736 Zhu, C., Kawamura, K., Fukuda, Y., Mochida, M., and Iwamoto, Y.: Fungal spores overwhelm biogenic
737 organic aerosols in a midlatitudinal forest, *Atmospheric Chemistry and Physics*, 16, 7497-7506,
738 10.5194/acp-16-7497-2016, 2016.
739



Table 1 Summary of the average BSOA tracers at the two sampling sites during the whole campaign.

Compounds	Mountain foot			Mountainside		
	Average	Daytime	nighttime	Average	Daytime	nighttime
Isoprene derived SOA tracers						
2-MGA ^a	28.6±14.7	35.7±16.8	21.7±7.4	16.2±8.4	19.5±9.4	12.9±5.6
2-methyltetrols						
2-Methylthreitol	24.0±10.1	24.7±10.4	23.3±9.8	32.1±22.6	28.6±20.9	35.6±23.7
2-Methylerythritol	49.7±22.4	51.9±23.2	47.7±21.3	66.6±46.4	57.3±41.8	76.0±48.9
subtotal	73.8±32.1	76.6±33.1	71.0±30.7	98.6±68.4	85.9±62.4	111.6±71.8
C₅-alkene triols^b						
cis-2-Me-1,3,4-THB ^b	20.1±12.8	20.1±12.7	20.1±12.9	21.8±17.9	19.2±15.4	24.4±19.8
3-Me-2,3,4-THB ^c	22.6±14.7	22.2±13.6	23.0±15.6	23.2±19.2	20.7±16.9	25.8±21.0
trans-2-Me-1,3,4-THB ^d	30.9±19.1	30.3±18.9	31.2±19.4	29.6±22.3	26.0±18.7	33.0±24.8
subtotal	73.5±46.4	72.6±44.9	74.3±47.7	74.5±59.2	65.9±50.8	83.2±65.5
3-MeTHF-3,4-diols						
trans-3-Me-THF-diol ^e	3.0±1.4	2.9±1.3	3.0±1.4	3.2±1.9	3.1±1.8	3.3±2.0
cis-3-Me-THF-diol ^f	3.8±1.5	3.7±1.5	3.8±1.5	4.7±3.7	4.4±3.4	5.0±4.0
subtotal	6.7±2.8	6.6±2.8	6.8±2.9	7.9±5.5	7.5±5.0	8.3±5.8
Total	182±81	191±83	173±77	197±126	178±114	216±135
α/β-pinene derived SOA tracers						
cis-pinonic acid	8.9±3.5	9.3±3.8	8.5±3.0	4.0±2.4	4.4±2.3	3.6±2.5
pinic acid	5.1±2.2	5.8±2.2	4.5±2.1	3.3±2.0	3.6±2.0	3.1±1.9
MBTCA ^g	26.3±14.1	30.1±13.6	22.7±13.6	19.4±12.9	21.2±13.7	17.6±11.8
3-HGA ^h	12.1±6.4	13.7±6.2	10.6±6.2	5.5±4.0	6.9±4.5	4.1±2.8
Total	52.4±23.1	59.0±22.4	46.2±22.0	32.3±20.0	36.1±21.0	28.4±18.0
β-caryophyllene derived SOA tracer						
β-Caryophyllinic acid	34.5±19.1	35.2±17.6	33.7±20.4	56.0±40.1	70.2±46.2	41.6±28.4

^a2-MGA: 2-methylglyceric acid;

^bcis-2-Me-1,3,4-THB: cis-2-Methyl-1,3,4-trihydroxy-1-butene;

^c3-Me-2,3,4-THB: 3-Methyl-2,3,4-trihydroxy-1-butene;

^dtrans-2-Me-1,3,4-THB: trans-2-Methyl-1,3,4-trihydroxy-1-butene;

^etrans-3-Me-TH-diol: trans-3-Methyltetrahydrofuran-3,4-diol;

^fcis-3-Me-TH-diol: cis-3-Methyltetrahydrofuran-3,4-diol;

^gMBTCA: 3-methyl-1,2,3-butanetricarboxylic acid;

^h3-HGA: 3-Hydroxyglutaric acid

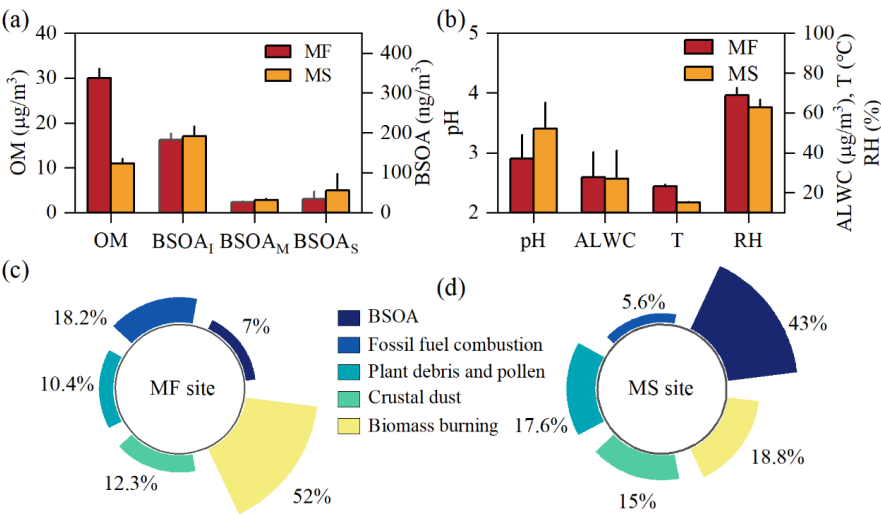


Figure 1 Comparisons upon chemical composition (a), meteorological conditions (b), and sources for OM (c and d) among two sampling sites. (OM concentration is converted by the OM/OC ratio measured in our previous (Wu et al., 2024))

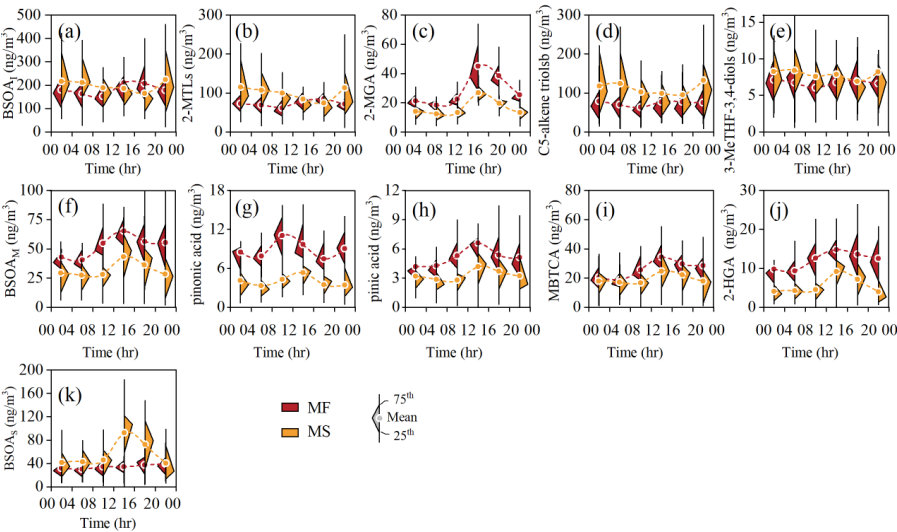
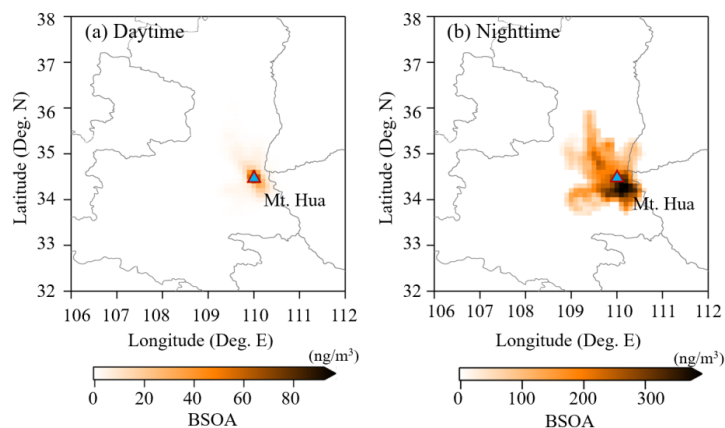


Figure 2 Diurnal variations in BOSA tracers among both sites. (a-e) isoprene-derived SOA tracer; (f-j) monoterpenes-derived SOA tracer; (k) β -caryophyllene -derived SOA tracer.



766



767

768 **Figure 3** A concentration-weighted trajectory (CWT) analysis for BSOA_I at MS site.

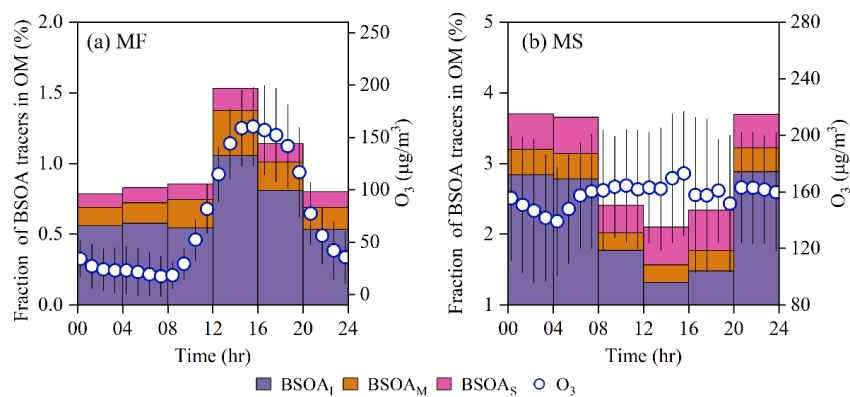
769

770

771

772

773



774

775 **Figure 4** Diurnal cycles of mass fraction of BSOA tracers in OM and O₃ at both
776 sampling sites.

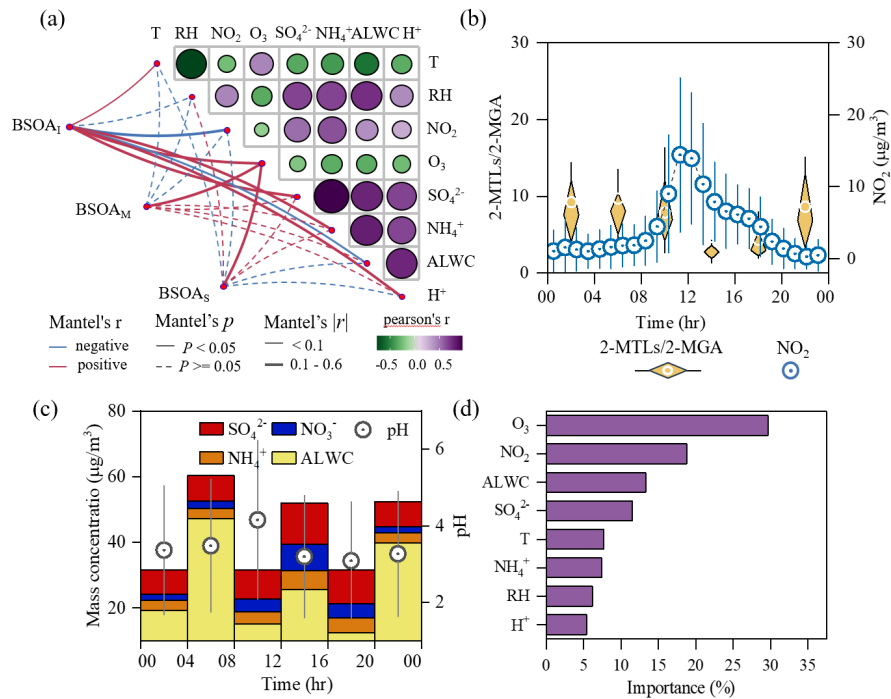


Figure 5 Formation of daytime isoprene-derived SOA in upper troposphere. **(a)** Mantel test between BSOA tracers and potential influencing factors at MS site; **(b and c)** Diurnal variations 2-MTLs/2-MGA ratio, pH, and the concentration of NO₂, SNA, ALWC at MS site; **(d)** Importance assessment for the key factors affecting the daytime isoprene-derived SOA at the MS site.

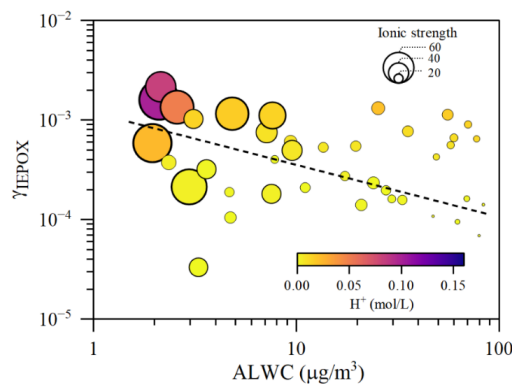


Figure 6 Reactive uptake (γ_{IEPOX}) as a function of ALWC during the daytime at MS site.